Paper # 070CO-0341 **Topic: Coal and biomass combustion and gasification**

8th US National Combustion Meeting
Organized by the Western States Section of the Combustion Institute
and hosted by the University of Utah
May 19-22, 2013.

Computational assessment of the effect of realistic intraparticle geometry on biomass heating rates and pyrolysis yields

R. W. Grout *K. Malhorta* *P. Ciesielski* *K. Gruchalla*
B. Donohoe *M. Nimlos*

National Renewable Energy Laboratory,
Golden, CO

The coupled heat transfer and chemical kinetics processes inside of a pyrolyzing biomass particle are simulated with realistic intra-particle geometry to investigate the effects of the cellular structure on char yields. Although the technology exists for deriving liquid fuels from biomass via pyrolysis oil, it is not currently cost-effective relative to competing fuel streams. DOE EERE's multi-year program plan articulates a goal to bring the estimated mature technology cost to produce gasoline and diesel blendstocks via thermochemical pathways down to $1.56 per gallon of total blendstock by 2017; decreasing the char residual during primary pyrolysis is a key improvement necessary to meet that goal. It is generally agreed that the residual char fraction is strongly dependent on the biomass heating rate; what is not well understood is the role of the biomass cellular structure on the localized heating rates and kinetics within a biomass particle. An unstructured finite-element analysis tool (DKSOLVE) is built upon *FEniCS*—an open source collection of tools for automating the solution of differential equations — to treat the diffusive transport and *Cantera* handle the pyrolysis reactions. Whereas previous attempts to account for intra-particle variation have considered only relatively simplistic geometries (e.g., radially symmetric cylinders and spheres) with low dimensional techniques, here full three-dimensional unstructured meshes are used to treat realistic geometries. Canonical geometries are created that typify key characteristics observed from experimental measurements. In this initial study, a lumped chemistry model for the primary pyrolysis kinetics is used to first validate the new code and computational techniques through comparison to earlier works considering spherical particles, followed by application to the complex geometry cases. It is found that the variations in heat transfer coefficients between the cell walls and lumen can lead to locally enhanced/degraded heating rates relative to a uniform particle and a corresponding non-uniformity in the residual composition. The foundation is formed for further work to examine the effects of secondary reactions occurring in pyrolysis gasses before they escape the biomass particle and to search for geometric modifications that improve yields and are achievable through practical pretreatments.

1 Introduction

Although the technology exists for deriving liquid fuels from biomass via pyrolysis oil, it is not currently cost-effective relative to competing fuel streams. DOE EERE's multi-year program plan articulates a goal to bring the estimated mature technology cost to produce gasoline and diesel blendstocks via thermochemical pathways down to $1.56 per gallon of total blendstock by 2017 [1]; decreasing the char residual during primary pyrolysis is a key improvement necessary to meet that goal.

It is generally agreed that the residual char fraction is strongly dependent on the biomass heating rate; what is not well understood is the role of the biomass cellular structure on the localized heating rates and kinetics within a biomass particle. The objective of this effort is to determine if the intracellular geometric structure plays a significant role in the final char quantities produced during a gasification or pyrolysis process.

To this end, an unstructured finite-element based tool (DKSOLVE) has been constructed using *FEniCS*—an open source collection of tools for automating the solution of differential equations [2]—to treat the diffusive transport and the *Cantera* [3] suite of chemical kinetics tools to treat the pyrolysis reactions. While the chemical mechanism, described in the following sections, is simplistic, the code framework can accept an arbitrary chemical kinetic network for both solid and gas phases.

After describing the mathematical formulation, we will proceed to discuss the validation and verification of the DKSOLVEcode to ensure that the implementation is correct and the results are meaningful, including analysis of a spherical particle. We will then move to discussion of the creation and analysis of a particle with canonical geometry reflecting the intracellular structure indicative of experimental observations.

2 Mathematical Formulation

The code developed for this effort—DKSOLVE—is built upon a combination of FEniCS for finite-element pde solution, SUNDIALS [7] to solve the set of coupled ODEs describing the chemistry at each node, and Cantera [3] to implement chemical reaction networks and thermodynamic properties. FEniCS [2] is a collection of tools (notably DOLFIN, [8, 9]) for the solution of variational problems using the finite-element method.

The primary solution quantities solved for are the density of each gas and solid phase species ρ_i and temperature. For ns species where the $\{1 \ldots ns_g\}$ species indicies refer to gas phase species and the $\{ns_g + 1 ... ns\}$ indicies refer to solid phase species the solid fraction is defined as:

$$\varepsilon_s = \frac{\sum_{(ns_g+1)}^{ns_s} \rho_i}{\sum_1^{ns} \rho_j}. \tag{1}$$

Properties are then given as mass-weighted average of solid and gas properties, i.e.,

$$\phi = \phi_g(1 - \varepsilon_s) + \phi_s \varepsilon_s, \tag{2}$$

where ϕ is an intensive property and ϕ_g, ϕ_s refer to the mean per-phase values that are computed independently using Cantera routines. The solid phase density varies only with composition and is computed based on molar volumes:

$$\rho_s \approx \frac{\sum X_k W_K}{\sum_k X_k V_k}. \tag{3}$$

Mass converted to the gas phase is assumed to escape instantly following the approach in earlier works [13]; gas phase species are not transported nor do they contribute to the reaction mechanism directly. They gas concentrations participate in the solution in only one fashion: when computing properties, and also therefore the solid volume fraction.

Energy conservation, including the enthalpies of reaction is:

$$\frac{\partial}{\partial t}(\rho C_p T) = \nabla \cdot (k \nabla T) + Q(t), \tag{4}$$

where $Q(t)$ is the enthalpy source term from the chemical reactions.

The unsteady heat transfer equation is integrated in time from t to $t + \Delta t$ using an operator-split approach with three stages:

Stage 1:

$$(\rho C_p T)^{\dagger} = (\rho C_p T)^t + \int_t^{t+\Delta t/2} Q(t) dt \tag{5}$$

$$\rho_i^{\dagger} = \rho_i^t + \int_t^{t+\Delta t/2} \frac{d\rho_i}{dt}(T) dt \tag{6}$$

Stage 2:

$$(\rho C_p T)^{\ddagger} = (\rho C_p T)^{\dagger} + (\Delta t) \nabla \cdot (k \nabla T)^{\ddagger}, \tag{7}$$

subject to convective boundary conditions:

$$k \nabla T \cdot \vec{n} = h_c (T_\infty - T) \tag{8}$$

or, in variational form,

$$\int_\Omega v (\rho C_p T)^{\ddagger} d\Omega + \int_{\partial\Omega} v (\Delta t)(h_c T)^{\ddagger} dS - \int_{\partial\Omega} v (\Delta t)(h_c T_\infty)^{\ddagger} dS + \int_\Omega (\Delta t) \nabla v \cdot (k \nabla T)^{\ddagger} d\Omega = \int_\Omega v (\rho C_p T)^{\dagger} d\Omega. \tag{9}$$

Stage 3:

$$(\rho C_p T)^{t+\Delta t} = (\rho C_p T)^{\ddagger} + \int_{t+\Delta t/2}^{t+\Delta t} Q(t) dt \tag{10}$$

Table 1: Kinetic parameters from Chan et al. [11]

#	Reaction	A	E_a
1	Biomass$(s) \rightarrow$ Gasses(g)	1.38E+08	140.3
2	Biomass$(s) \rightarrow$ Vapors(g)	2.00E+08	133.1
3	Biomass$(s) \rightarrow$ Char(s)	1.1E+07	121.3

$$\rho_i^{t+\Delta t} = \rho_i^{\dagger} + \int_{t+\Delta t/2}^{t+\Delta t} \frac{d\rho_i}{dt}(T^{\ddagger})dt \tag{11}$$

In the present formulation there is no species transport by advection or diffusion in either phase. This has implications that there is no enthalpy transport by diffusing species or advection in the lumen; enthalpy transport through the lumen is purely diffusive. Notionally, this is treating the lumen as stagnant gas, perhaps reasonable given the small dimension of the lumen regions, but studying the effects of relaxing this assumption is certainly an avenue for future work.

2.1 Chemical Kinetics

We use the same simple kinetic scheme utilized by Al-Haddad et al. [10] with the three competitive reactions and the coefficients suggested by Chan et al. [11] for cellulose/wood as listed in Table 1.

The evolution of the mass of the i^{th} of ns species is written in the form:

$$\frac{d\rho_i}{dt} = A_i e^{-E_i/(R_g T)} a_w(t), \tag{12}$$

where the inter-species coupling comes through the concentration of unreacted wood $\rho_w(t) = \rho_N(t)$:

$$\frac{d\rho_w}{dt} = -\sum_{i=ng+1}^{ns} \frac{d\rho_i}{dt}. \tag{13}$$

The solid phase activities—the method is general although the specific mechanism used here requires only the activity of wood—are the solid phase mass concentrations weighted by the solid fraction:

$$a_k = Y_k \rho_s \varepsilon_s. \tag{14}$$

3 Results

3.1 Validation and Verification

Three basic tests of the DKSOLVEanalysis tool are considered here: comparison to an analytic solution for transient heating of a spherical particle (to test correctness of the solution to the heat

transfer equation), a verification that the total mass of a particle is constant (to test the implementation of the chemical kinetics) and finally, analysis of a spherical reacting particle to ensure that the trends in yield vs. heating rate are consistent with the literature (as an overall validation of the code).

Transient heat conduction in spherical particle An inert, non-reacting spherical particle with constant composition subject to convective heating has an analytical solution. For a sphere of radius of 800 microns initially at $T_0 = 400$k in an ambient temperature of $T_\infty = 1200$k and other salient parameters as given in Table 2, a one-term approximation to the analytical solution valid for non-dimensional time $\tau > 0.2$ is given by [12]:

$$\theta_{\text{sphere}} \approx A_1 e^{-\lambda_1^2 \tau} \frac{\sin\left(\lambda_1 \frac{r}{r_0}\right)}{\lambda_1 \frac{r}{r_0}}, \tag{15}$$

where λ_1 and A_1 are tabulated functions of the Biot number:

$$Bi = \frac{hr_0}{k} = 2.7586 \Rightarrow A_1 = 1.588, \lambda_1 = 2.226, \tag{16}$$

and θ, τ are the non-dimensionalized temperature difference and time:

$$\theta \equiv \frac{T - T_0}{T_\infty - T_0}; \quad \tau \equiv F_0 = \frac{\alpha t}{r_0^2}. \tag{17}$$

Table 2: Parameters used in present simulations

Property	Wood	Char	Voids (air)
C_p[J/kg/k]	15000.35	9850.35	10000.35
ρ[kg/m^3]	1000.0	720.0	1.20
k[W/m/k]	0.29	0.10	0.0257
h_c[W/m^2/k]	1000	1000	1000

The test problem is formulated by supplying DKSOLVEwith a mesh of a sphere and running the code with all chemical reactions suppressed. A radial profile is extracted at several points in time and compared to the analytic solution in Figure 1.

We observe overall quantitative agreement between the DKSOLVEresult and the analytic solution. The largest disagreement is at the earliest time, where the one-term approximation to the analytic solution is not exact: some difference is expected due to that approximation rather than the DKSOLVEsolution. At later times agreement is excellent. The tight grouping of the solutions for $t = 10$ for various mesh sizes and time increments suggest the solution is time and space resolved.

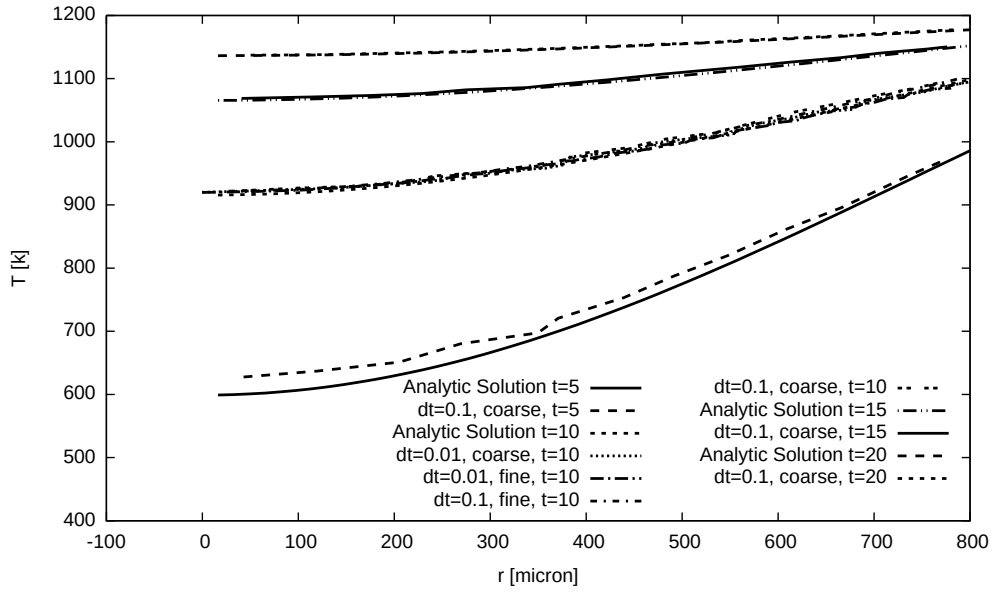

Figure 1: Comparison to analytic solution for sphere with 800 micron radius

Mass Conservation To test that the implementation conserves mass globally in the presence chemical reaction, the code is run with chemical reaction enabled and the evolution of volume-integrated total mass as well as the individual solid and gas phase mass evolution is output. The results are shown as a function of normalized time in Figure 2. The time is nondimensionalized by t^*, defined as the time when the non-dimensional temperature defect is less than 5%:

$$\frac{T_\infty - T_{\min}}{T_\infty - T_0} < 0.05, \tag{18}$$

indicating that the particle temperature has approximately reached the ambient temperature. Reassuringly, the solution reaches steady state near t^* and mass is globally conserved.

Effect of heating rate on yield for a spherical particle Spherical particles have been analysed with several different methods using the same or similar chemistry, e.g., references [13, 14, 15]. Running the simulation to steady state for the same spherical particle used for the transient heating test, but this time with chemical reaction enabled, we can perform a parametric study on the effect of the convective heat transfer coefficient h_c and, indirectly, on the resulting particle heating rate. The integration of the mass density of each species (gas, vapors, char) over the volume at the end of the simulation, normalized by the wood mass at the start of the simulation, is shown in Figure 3. As expected from the literature, the trend is shown that increasing the heating rate corresponds to increased gas and vapor fraction along with decreased char residual.

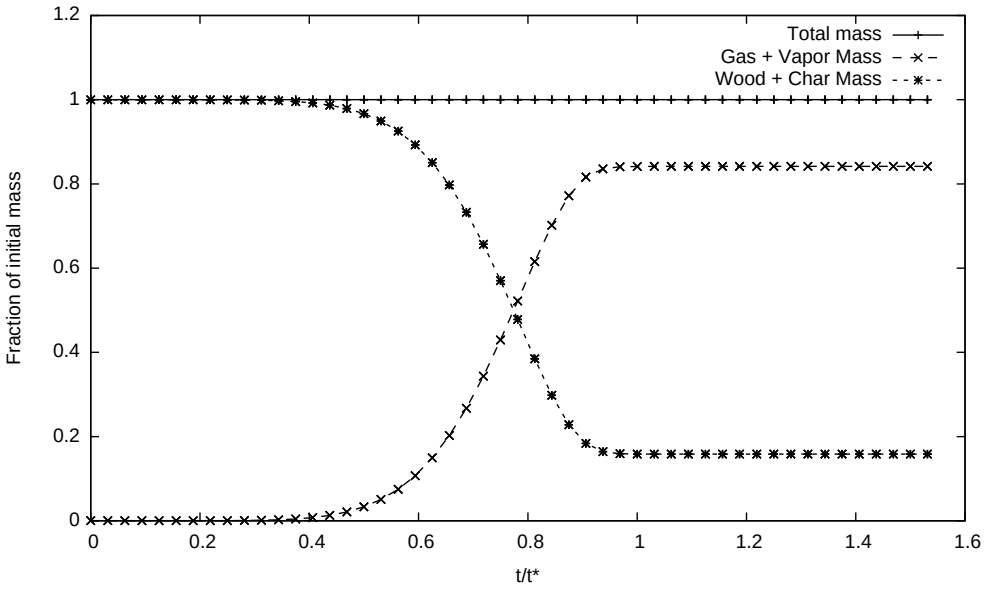

Figure 2: Total, gas and solid phase volume mass totals over time for 8 lumen geometry

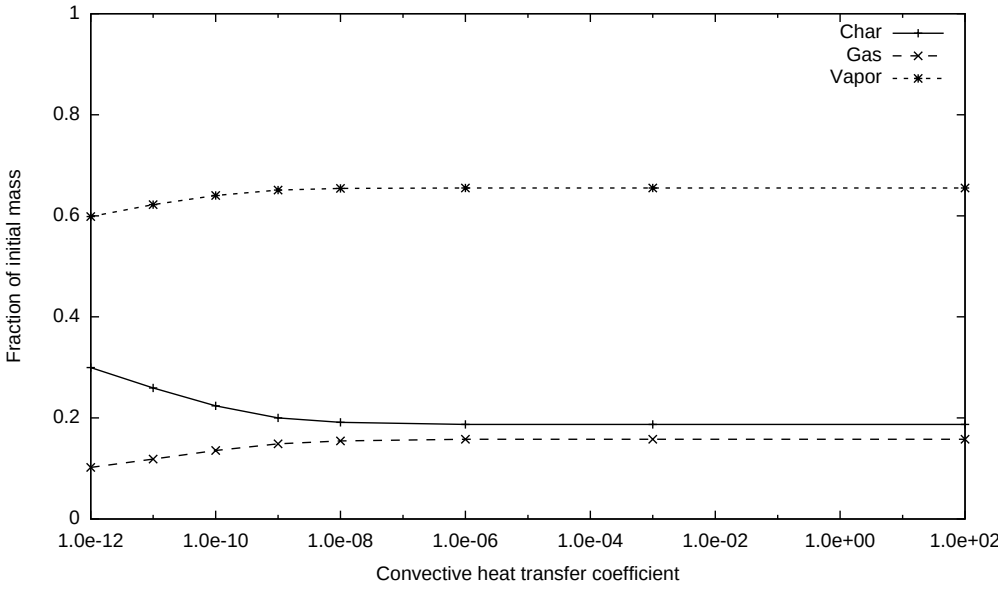

Figure 3: Effect of convective heat transfer coefficient on ultimate yield

3.2 Simulation of Canonical Particle Geometry

Moving now to our primary interest—a particle with cellular structure, we will first describe the technique for developing the computational mesh, followed by the results of the simulation.

Table 3: Parameters for synthetic canonical geometry

Lumen tangential diameter	35.3 ± 5.9
Lumen radial diameter	35.07 ± 6.4
Cell wall tangential thickness	2.99 ± 0.58
Cell wall radial thickness	3.16 ± 0.70

Canoical geometry creation In order to construct a *FEniCS*-compatible mesh, we developed a a custom unstructured mesh generation workflow starting with 3D image data as input. For this effort, the workflow begins with a synthetic three-dimensional image representing the canonical geometry, but our intention is that the same workflow can also be fed with data obtained from experimental measurements directly (e.g., extruded from 2D spectroscopy or 3D CT reconstructions). A threshold is used to separate the 3D image into two materials: cell wall and lumen. Triangulated bounding surfaces approximating the interfaces between these materials are computed with a generalized marching cubes algorithm [16]. These surfaces are then remeshed to both simplify the triangulation and improve triangle quality using a Llyod relaxation to make isotropic vertex placements [17]. The advancing front method [18, 19] is applied to fill each volumetric region defined by the surfaces with tetrahedra.

The synthetic three-dimensional image is generated using a mathematical algorithm that was developed to generate simulation geometries representative of cell wall microstructure based on experimentally measured parameters including cell lumen radial and tangential diameters, cell wall radial and tangential thicknesses, and pit density. For this study, parameters measured for spruce wood [20, 21] were used; these data are summarized in Table 3. With a user defined volume space, a set of nodes was initialized as solid cell wall. Then, a possible set of lumen tangential and radial diameters was generated over a normal distribution of the measured mean and standard deviation parameter values. The algorithm finds the maximum number of lumen (in the x and y axis) that can fit in the specified volume space. Similarly, the lumen lengths are normally distributed and start at random points in the z axis. Any node found on or within a lumen is defined as void space.

Effect of heating rate on yield When the canonical particle is heated and reacted until steady-state is reached, the total mass of each species at steady state is shown in Figure 4. The canonical particle results follow the same trends as the spherical particle, although the dependence on h_c is less pronounced. However, the canonical particle is somewhat smaller than the spherical particle considered earlier. For the spherical particle the effect is less pronounced at higher heating rates, and shrinking the particle moves the process towards faster heating.

Intraparticle variation in heating rates and kinetic process Looking inside the particle at an intermediate time as well as at steady state, we see that there is some evidence that there is variation in heating rates and the ultimate char yield throughout the particle. The intermediate temperature variation is similar to what we would expect for a solid particle, yet the structure of the particle is clearly visible in the volume rendering of the temperature at the top right of Figure 5. For

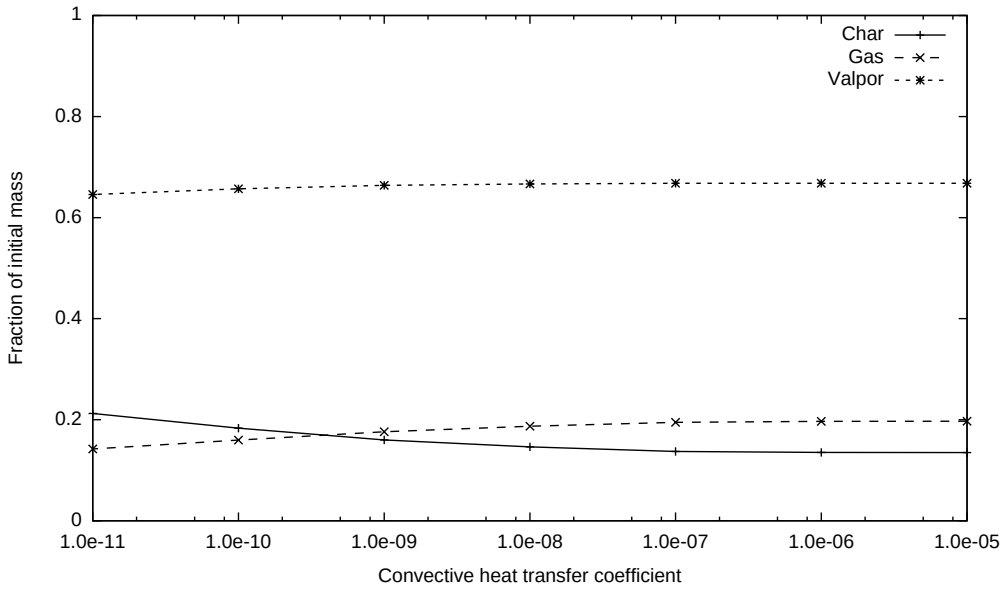

Figure 4: Effect of convective heat transfer coefficient on ultimate yield — canonical particle with 8 lumen volumes

reference, the particle geometry is shown in the top left, where the computational mesh is overlaid on the solid fraction.

Even after pyrolysis is complete, the char distribution (Figure 5, bottom), within the particle is clearly geometry dependent with more char near the outside of the particle and variations that follow the contours of the solid geometry.

4 Conclusions

In this initial study the newly developed code DKSOLVEwas used with a lumped chemistry model for the primary pyrolysis kinetics to validate the code and computational techniques through comparison to earlier works considering spherical particles, followed by application to the complex geometry cases. The complex geometry was constructed using a workflow equally applicable to either experimentally measured or synthesized canonical geometry. For the canonical geometry considered here, geometric variations in heat transfer coefficients between the cell walls and lumen lead to local excursions in temperature associated with the intracelular geometry. Although the temperature excursions are slight, a noticeable geometric variation in char formation is observed. This suggests scope for future work in a number of areas. Increasing geometric complexity and realism as well as improved treatment of the gas phase to consider transport and secondary reactions are both indicated. While it is attractive to consider geometry derived directly from microscopy, exploring a parametric study of the effect of wall structure based on the parameters of the synthetic geometric model may also prove fruitful.

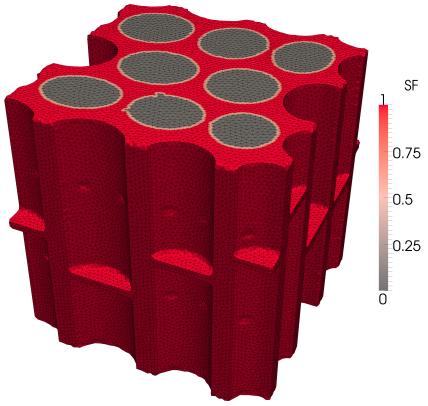

Initial solid fraction and mesh

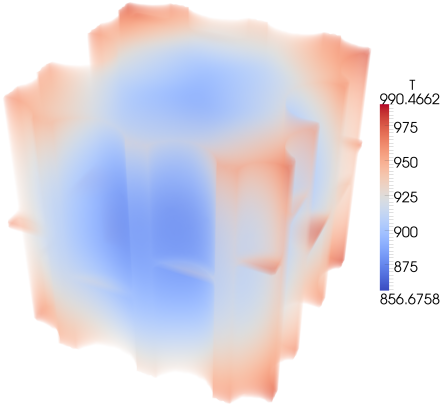

Temperature at $t/t^* = 0.625$

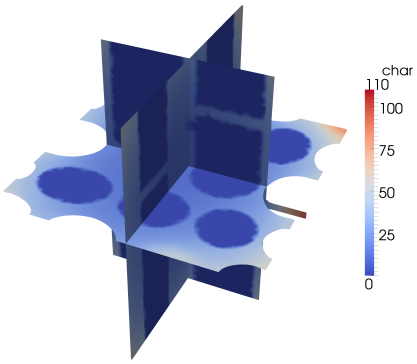

Char fraction at $t/t^* = 0.625$

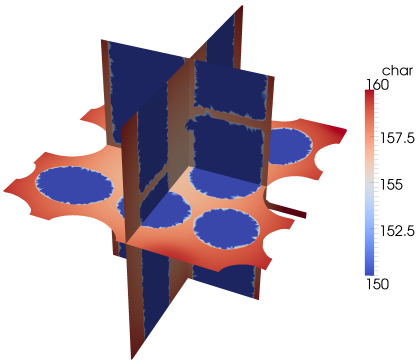

Char fraction at $t/t^* = 1.5625$

Figure 5: Temperature and Char mass concentration during conversion and after all wood is converted.

Acknowledgments

This work is supported by United States Department of Energys Bioenergy Technology Office, under Contract No. DE-AC36-99GO10337 with the National Renewable Energy Laboratory.

References

[1] *Biomass multi-year program plan*. Department of Energy Office of Energy Efficiency & Renewable Energy, 2011.

[2] Anders Logg, Kent-Andre Mardal, Garth N. Wells, et al. *Automated Solution of Differential Equations by the Finite Element Method*. Springer, 2012.

[3] D. Goodwin. Cantera: An object-oriented software toolkit for chemical kinetics, thermodynamics, and transport processes. Available online: http://code.google.com/p/cantera, 2012.

[4] J.M. Davis Y. Lin, J. Cho and G. W. Huber. *Chem. Eng. Sci*, 74 (2012) 160–171.

[5] Anup Kumar Sadhukhan, Parthapratim Gupta, and Ranajit Kumar Saha. *Journal of Analytical and Applied Pyrolysis*, 81 (2008) 183–192.

[6] N. Gierlinger and M. Schwanninger. *Plant Physiology*, 140 (2006) 1246–1254.

[7] A. C. Hindmarsh, P. N. Brown, K. E. Grant, S. L. Lee, R. Serban, D. E. Shumaker, and C. S. Woodward. *ACM Transactions on Mathematical Software*, 31 (2005) 363–396.

[8] Anders Logg and Garth N. Wells. *ACM Transactions on Mathematical Software*, 37 (2010) journal.

[9] Anders Logg, Garth N. Wells, and Johan Hake. *DOLFIN: a C++/Python Finite Element Library*, chapter 10. Springer, 2012.

[10] M. Al-Haddad, E. Rendek, J.-P. Courriou, and G. Mauviel. *Energy and Fuels*, 24 (2010) 4689–4692.

[11] Wai-Chun R. Chan, Marcia kelbon, and Barbara B. Krieger. *FUEL*, 64 (1985) 1505–1513.

[12] Frank P. Incropera and David P. DeWitt. *Introduction to Heat Transfer*. John Wiley & Sons, Inc., second edition, 1990.

[13] M Al-Haddad, E Rendek, J P Corriou, and G Mauviel. *Energy Fuels*, 24 (2010) 4689–4692.

[14] Woon Chan Park, Arvind Ateya, and haoward R. Baum. *Combustion and Flame*, 157 (2010) journal.

[15] Enrico Grieco and Giancarlo Baldi. *Chem. Eng. Sci*, 66 (2011) 650–660.

[16] *A generalized marching cubes algorithm based on non-binary classifications.* Preprint SC-97-05. ZIB, 1997.

[17] Michael Zilske, Hans Lamecker, and Stefan Zachow. Adaptive remeshing of non-manifold surfaces. In *Eurographics 2008 Annex to the Conf. Proc.*, pages 207–211, 2008.

[18] Rainald Löhner and Paresh Parikh. *International Journal for Numerical Methods in Fluids*, 8 (1988) 1135–1149.

[19] H. Jin and R. I. Tanner. *International Journal for Numerical Methods in Engineering*, 36 (1993) 1805–1823.

[20] P Trtik, J Dual, D Keunecke, D Mannes, P Niemz, P Stähli, A Kaestner, A Groso, and M Stampanoni. *Journal of structural biology*, 159 (2007) 46–55.

[21] Y. Sano, H. Morris, H. Shimada, L. P. Ronse De Craene, and S. Jansen. *Annals of Botany*, 107 (2011) journal.